Log Number: 000

OECD/NRC NUPEC PSBT BENCHMARK: SIMULATION OF THE STEADY-STATE SUB-CHANNEL TEST-CASE WITH NEPTUNE CFD

C. Baudry¹, M. Guingo¹, A. Douce¹, J. Laviéville¹, S. Mimouni¹, M. Boucker¹
¹ EDF R&D, Fluid dynamics, Power Generation and Environment Dpt., 6, quai Watier,
Chatou 78400, France

<u>cyril.baudry@edf.fr</u>, <u>mathieu.guingo@edf.fr</u>, <u>alexandre.douce@edf.fr</u>, <u>jerome-marcel.lavieville@edf.fr</u>, <u>stephane.mimouni@edf.fr</u>, <u>marc.boucker@edf.fr</u>

Abstract

In this paper, we present numerical results obtained with the multifield CFD code NEPTUNE_CFD in the framework of the OECD/NRC PWR Subchannel and Bundle Tests (PSBT) international benchmark, focusing on the simulation of five selected runs of the steady-state subchannel exercise. The propagation of the estimated experimental uncertainties on the simulations results is investigated, as well as the mesh sensitivity of the axial evolution of the mean void-fraction by using three grid levels. Last, calculation results using a devoted model for the bubble-size distribution are presented.

1. Introduction

The OECD/NRC PWR Subchannel and Bundle Tests (PSBT) benchmark is an international project endorsed by the OECD/NEA and supported by US NRC and METI (Japan), in which a large experimental database of void-fraction measurements performed under PWR thermal-hydraulic conditions in different geometric configurations (different types of isolated subchannels or rod bundle) has been made available to the participants. One of the purposes of this benchmark is to provide experimental data that can be used for the validation of numerical models of void-fraction distribution over a wide range of operating conditions, and for the development of novel approaches.

This paper aims at presenting the simulations carried out with the multifield computational fluid dynamics (CFD) code NEPTUNE_CFD [1] for one of the exercises of this benchmark, namely the steady-state single subchannel. For this exercise, three main results are asked from the participants:

- a numerical calculation of the cross-section void fraction at a given elevation,
- a 2D view of the void-fraction distribution in this section.
- the evolution of the cross-section averaged void-fraction with respect to the elevation.

Following the NEA/CSNI Best Practice Guidelines, a mesh sensitivity analysis is performed on three grid refinements, and the influence of the experimental uncertainties on the numerical results is assessed. As a first step, the standard set of parameters of the code is applied, with in particular the use of a second-order (Reynolds stress) turbulence model, as well as a constant, predetermined bubble diameter. The impact of a more detailed description of the bubble-size distribution is also presented.

1.1 Main features of the NEPTUNE CFD code

NEPTUNE_CFD is a 3D, multifield CFD code developed in the framework of the NEPTUNE project, financially supported by CEA (Commissariat à l'Energie Atomique et aux Energies Alternatives), EDF, IRSN (Institut de Radioprotection et de Sûreté Nucléaire) and AREVA-NP. It is mainly devoted to the study and the simulation of nuclear reactor applications involving multiphase flows, such as two-phase Pressurized Thermal Shock (PTS) and Departure from Nucleate Boiling (DNB) applications. The need to simulate PTS applications have led in particular to the development and the numerical implementation of specific methods of interface detection for free surface flows [2].

The code follows the classical multifield one-pressure formulation [3], and the spatial discretization is a full unstructured finite-volume approach with a collocated arrangement of all-variables. The numerical algorithm used is a semi-implicit, pressure-based method where the system of equations is solved in two major fractional steps: first, a prediction of the velocities based on the momentum equations; then, the coupling between phase fraction, pressure and energy through mass and energy equations and a simplified form of momentum equations [4].

2. Experimental configuration of the steady-state subchannel exercise

The test facility of the steady-state subchannel exercise represents one of the subchannel types found in PWR assembly. The effective heated length is 1.555 m, while the measurement of the void fraction takes place at 1.4 m from the bottom of the heated section. The void fraction is measured by using the chromo-tomography (CT) technique, which also gives the local distribution of the time-averaged void-fraction at the measuring section.

After discussion between participants of the PSBT benchmark who intended to simulate the exercises by following a CFD approach, five runs have been selected to be more precisely analysed:

- the run whose operating conditions are the closest to PWR normal conditions (reference 1.2211),
- two runs with a higher inlet temperature and a relatively low wall heat flux (references 1.2223 and 1.2237),
- two runs differing only by the value of the inlet temperature (references 1.4325 and 1.4326), with a lower heat flux and a lower pressure than run 1.2211.

The value of the controlling parameters of the runs and the cross-section averaged void-fraction measurements are summarized in Table 1. Furthermore, the estimated uncertainties on the flow parameters and on the void fraction measurement provided by the experimentalists are given in Table 2. It can be observed that the 1.2211 test is the only selected run in subcooled conditions (with a negative thermal equilibrium quality at the measuring section).

Reference of the run	1.2211	1.2223	1.2237	1.4325	1.4326
		11-0		22.4	20.2
Outlet pressure (bar)	147.2	147.2	147.4	98.4	98.2
Inlet temperature (°C)	295.4	319.6	329.6	253.8	268.8
Inlet mass flow rate (kg/m²/s)	3030.6	3030.6	3036.1	1397.2	1394.4
Wall heat flux (kW)	90	69.8	60	59.8	59.8
Equilibrium quality	-0.04	0.04	0.08	0.05	0.11
Averaged void fraction	0.04	0.31	0.44	0.34	0.53
Averaged fluid density (kg/m ³)	610	456	390	478	353

Table 1 Summary of the characteristics of the 5 selected test-cases. In bolded font, the run whose conditions are the closest of the PWR conditions.

	Estimated experimental uncertainties
Pressure	1%
Inlet temperature	1 °C
Mass flow rate	1.5%
Wall heat flux	1%
Averaged void fraction (1σ)	0.03 (CT measurement)

Table 2 Summary of the estimated experimental uncertainties on the controlling parameters of the test-case and on the measured void fraction.

3. Physical modelling

The turbulence of the liquid phase is modelled using a second-order, RANS model (Reynolds Stress Model) [5] including bubble-induced turbulence effects, whereas a turbulent dispersion model is applied on the gas phase [6]. The interfacial transfer of momentum is considered as the sum of different contributions, namely the drag force (modelled by using the correlation developed by Ishii [7]), the added mass force (by using the expression of Zuber [8]) and the formulation of the lift force proposed by Tomiyama [9]. As a general feature of the NEPTUNE_CFD code, no flow-regime map is used, as the flow is regarded as bubbly. No parameter-tuning with respect to the experimental results has been attempted.

At the heating wall, the heat transfer model is an extension of the approach of Kurul *et al.*[10] (often referred to as the RPI model) consisting in splitting the heat flux into three terms: one heating the liquid phase in contact with the wall, one responsible for the bubble generation and the last one arising from the arrival of liquid water at the wall, caused by bubble departure (the so-called "quenching" flux). When the void fraction in the boundary cells is sufficiently high, a fourth flux is introduced to take into account the convective heat transfer transmitted to the vapour.

For the first series of calculations, a constant diameter for the bubbles has been taken equal to 0.3 mm, based on previous experimental observations carried out in PWR conditions [11]. It can be thus expected for this modelling choice to behave more satisfactorily for runs with a relatively low void-fraction (i. e. where coalescence and fragmentation phenomena can be neglected). As a second step, the influence of a more refined description of the bubble-size distribution has been studied by performing simulations using the interfacial area model of Yao & Morel [13], which has been validated in PWR conditions in a vertical duct geometry.

4. Computational strategy

4.1 Time convergence

In order to reach the steady state, a transient algorithm is used in NEPTUNE_CFD. The time step chosen is time-dependent, with a maximal CFL number set to 1 for stability reasons and convergence of the iterative numerical algorithm.

4.2 Characteristics of the grids

Following the NEA/CSNI Best Practice Guidelines, three grids with different refinements have been used for this study. Their main features are recapitulated in Table 3; cross-section views of the grids are proposed in Figure 1 to Figure 3. The normalized wall-normal distance of the boundary-cells centres ranges from approximately 75 (run 1.4326, grid level 3) to approximately 320 (run 1.2211, grid level 1), supporting the use of a high-Reynolds formulation of a second-order RANS turbulence model.

	Grid level 1	Grid level 2	Grid level 3
Total number of cells	154,812	602,040	1,561,152
Number of cells in the axial direction	400	520	520
Number of cells in a cross-section	388	1160	3008
Cell size in the axial direction	4 mm	3 mm	3 mm
Distance-to-wall of the centres of the boundary cells	0.25 mm	0.15 mm	0.1 mm

Table 3 Characteristics of the grids used in the simulations.

It can be seen that the refinement factor from grid level 1 to grid level 3 is approximately equal to 3 following two perpendiculars belonging to a cross-section, and 1.3 in the axial direction.

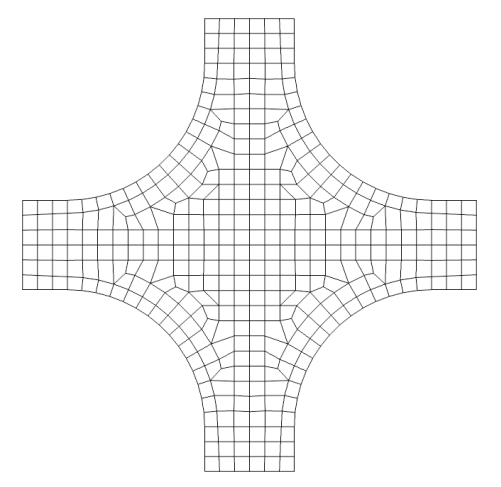


Figure 1 Cross-section view of grid level 1.

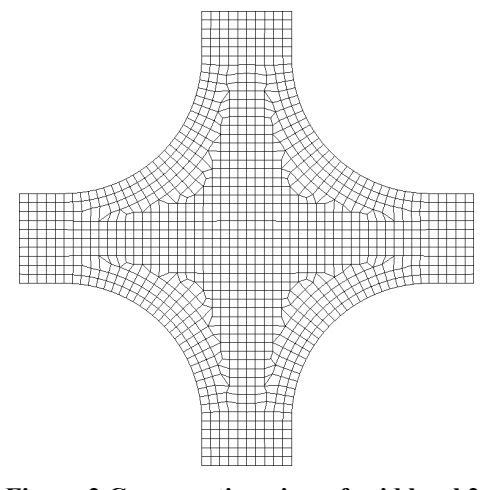


Figure 2 Cross-section view of grid level 2.

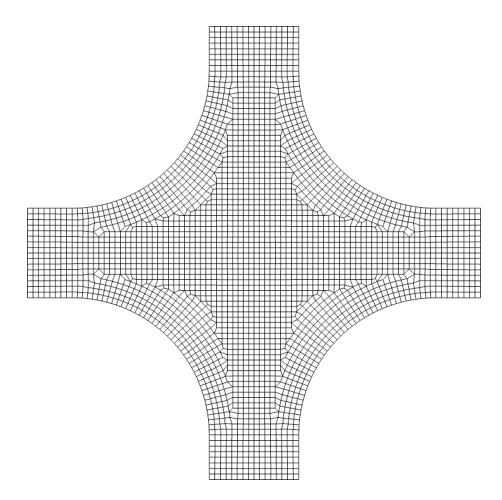


Figure 3 Cross-section view of grid level 3.

4.3 Boundary and initial conditions

The profiles of the inlet velocities and turbulent variables (Reynolds stresses and mean dissipation) have been calculated before-hand through devoted calculations, so as to get developed flow profiles.

The procedure followed for these calculations amounts to calculating a case without thermal power in an infinite channel of the same cross section; and then selecting the profiles of the variables where they do not vary anymore. The initial conditions on the velocities, the temperature and the turbulent variables are taken equal to the inlet conditions.

5. Results obtained and discussions

5.1 Mesh sensitivity analysis

The calculations have been carried out on 64 or 128 processors on a EDF R&D cluster (Xeon X5570 2.93 GHz Infiniband). The time to reach the steady state represents approximately 2 seconds of "physical" time. First, calculations were run under nominal conditions on the three grid levels to investigate the grid sensitivity of the results. The values of the cross-section averaged void fraction at the 1.40-meter section are summarized in Table 4.

	1.2211	1.2223	1.2237	1.4325	1.4326
Exp. values	0.04	0.31	0.44	0.34	0.53
Grid level 1	0.09	0.25	0.35	0.45	0.61
Grid level 2	0.10	0.26	0.36	0.42	0.60
Grid level 3	0.11	0.26	0.36	0.40	0.61

Table 4 Summary of the cross-section averaged void fraction obtained on the three grid levels.

It can be observed that simulations performed on grid level 1 give void-fraction values reasonably close to those obtained on grid level 3; the most significant discrepancy (0.45 against 0.40) being obtained for run 1.4325.

5.2 Results at the measuring section

Concerning the comparison with the experimental value (for grid level 3):

- for run 1.2211 (subcooled), the simulations overestimate the void-fraction by 0.07;
- for runs 1.2223 and runs 1.2237 (high inlet temperature and low wall heat flux), the simulations underestimate the experimental void-fraction by 0.05 to 0.09;
- for runs 1.4325 and 1.4326 (low pressure), the void-fraction is overestimated by 0.05 to 0.08.

On average, the deviation between numerical results and experimental data is then of the order of 0.06 void-fraction units; and consequently more visible on the subcooled run (1.2211).

5.3 Axial evolution of the flow

The axial evolution of the cross-section averaged void-fraction for the five runs are presented in Table 5, as well as the axial evolution of the wall temperature at a given location of a heating wall (see Figure 4), for the calculations performed on grid level 2.

It can be seen that for every run (except the subcooled run 1.2211), vapour is generated right from the start of the heated section. Furthermore, concerning runs 1.2223, 1.2237 and 1.4325, a change of the slope in the evolution of the mean void fraction is visible, respectively for an elevation approximately equal to 0.9 m, 0.55 m and 0.9 m. This change occurs at the same elevation as an increase of the wall temperature, indicating the beginning of the fully-developed sub-cooled boiling (FDB) [12].

For run 1.4326 (with the highest predicted and experimental void fraction), different regimes are observed:

- from the bottom of the sub-channel to approximately 0.5 m, the mean void fraction is rising slowly, corresponding to the partial sub-cooled boiling regime;
- from 0.5 m up, the void-fraction rises more rapidly, corresponding to the FDB regime. The evolution of the liquid temperature and of the saturation temperature is plotted in Figure 10, making it possible to locate the beginning of the saturated boiling regime at an elevation equal to 1.3 m;
- finally, for the last 5 cm of the domain, the wall temperature jumps from 605 K to 665 K: in this region, the calculated near-wall void-fraction exceeds 0.8, which is the threshold value used in the code to switch continuously from the nucleate boiling to a pseudo-film boiling. In this model, the totality of the imposed heat flux is transferred to the vapour (rising its temperature above saturation), therefore bringing about a drop of the heat transfer coefficient. Let us note that this model is not yet considered as validated.

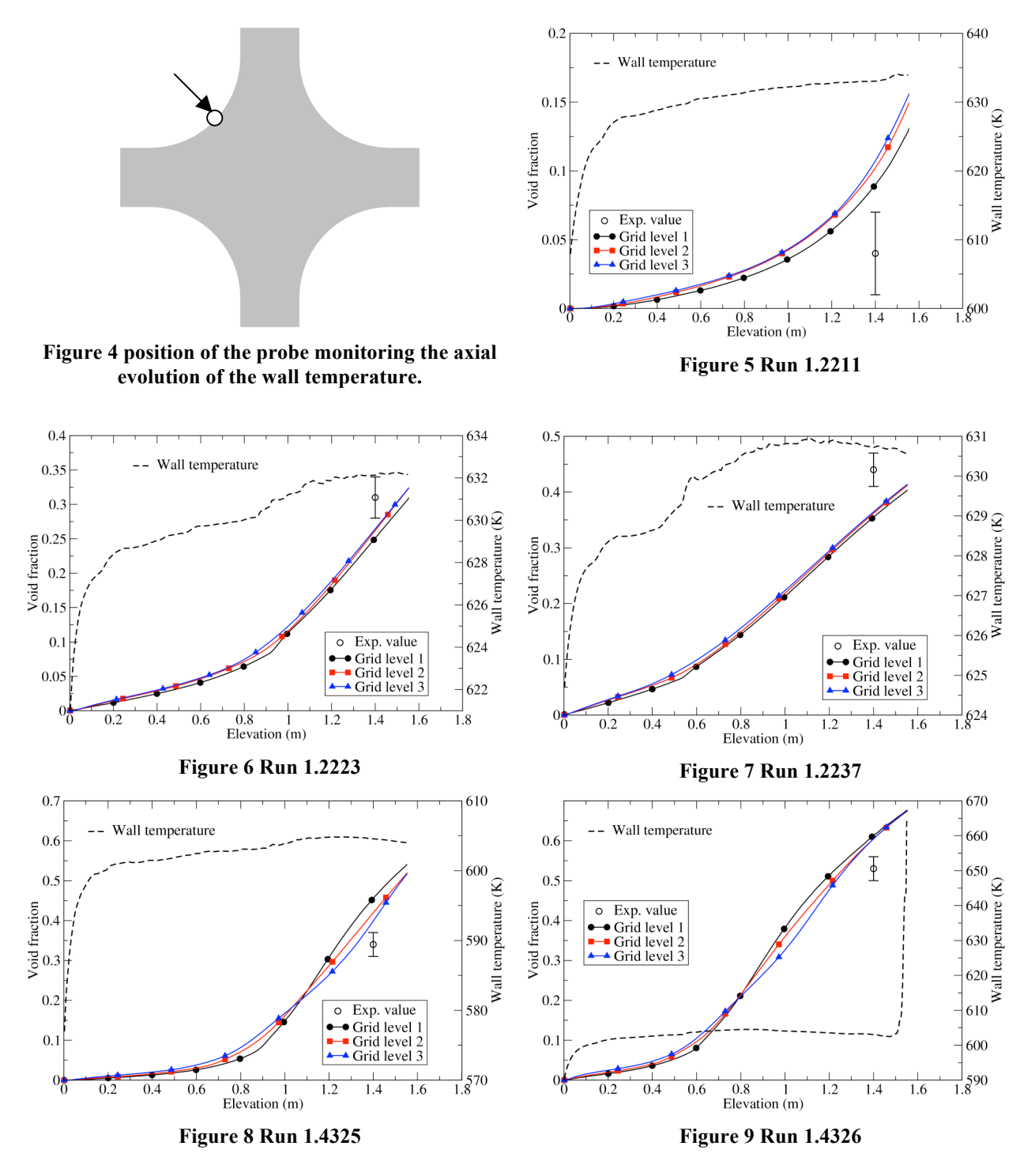


Table 5 Evolution of the cross-section averaged void-fraction with respect to the elevation for the five selected runs.

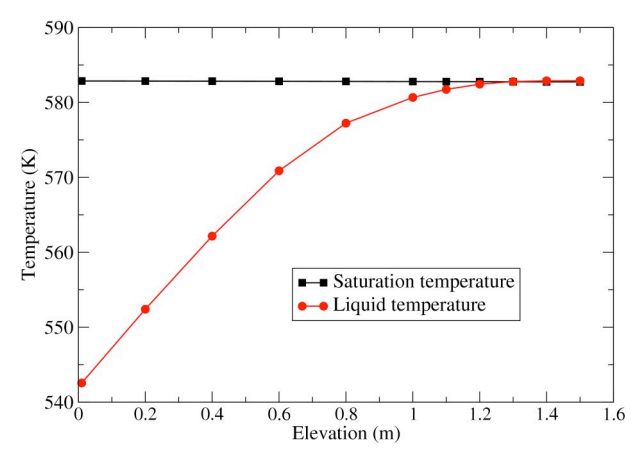


Figure 10 Calculated evolution of the liquid temperature and the saturation temperature for run 1.4326 (grid level 2) as a function of elevation.

5.4 Propagation of the experimental uncertainties

As the estimated uncertainties on the controlling parameters of the flow are provided (see Table 2), it is interesting to analyse the effects of these uncertainties on the simulations. For this purpose, a series of calculations have been performed, in which one of the controlling parameters is taken equal to its nominal values plus or minus the value of the relative uncertainties, the other parameters remaining fixed to the nominal values. This procedure makes it possible to study the effect of one uncertainty independently from the others. In order to keep a reasonable time-to-result, the coarsest grid has been used (grid level 1). The results obtained for the void fraction are recapitulated in Table 6.

	1.2211	1.2223	1.2237	1.4325	1.4326
Experimental values	0.04	0.31	0.44	0.34	0.53
Nominal calc. values	0.09	0.25	0.35	0.45	0.61
Pressure + 1%	0.082	0.235	0.337	0.441	0.603
Pressure – 1%	0.097	0.274	0.378	0.467	0.624
Inlet Temp. + 1 K	0.096	0.272	0.377	0.466	0.623
Inlet Temp 1 K	0.083	0.236	0.337	0.442	0.604
Mass flow rate + 1.5%	0.084	0.245	0.35	0.438	0.602
Mass flow rate – 1.5%	0.096	0.263	0.365	0.469	0.623
Wall heat flux + 1%	0.094	0.26	0.362	0.464	0.621
Wall heat flux – 1%	0.085	0.248	0.352	0.443	0.606

Table 6 Effects on the experimental uncertainties on the simulations.

These series of calculations show that for a relatively small variation of any parameter, the result on the averaged void-fraction is modified by approximately 0.01, whatever its absolute value. Consequently, the relative impact on the void-fraction value of a single parameter variation is more visible on the subcooled case (approximately 10%), i. e. the run that shows the lowest void-fraction value. Then, two additional series of calculations have been carried out: for each series, the set of parameters *expected to give the highest or the lowest value of the averaged void-fraction has been chosen*. The results obtained are reported in Table 7.

	1.2211	1.2223	1.2237	1.4325	1.4326
Experimental values	0.04	0.31	0.44	0.34	0.53
Nominal calc. values	0.09	0.25	0.35	0.45	0.61
Pressure – 1% Inlet Temp. + 1 K Mass flow rate – 1.5% Wall heat flux + 1%	0.126	0.31	0.40	0.50	0.65
Pressure + 1% Inlet Temp 1 K Mass flow rate + 1.5% Wall heat flux - 1%	0.078	0.20	0.30	0.40	0.58

Table 7 Calculated values of the cross-averaged void fraction with two sets of parameters.

These simulations show that taking the two "opposite" sets of parameters give numerical results that may span on a range quite wide: for instance, for run 1.4325, void-fraction value varies on a 0.1-wide interval, representing approximately 20% of the nominal value. The impact is more visible for run 1.2211, where a calculated 0.05-wide variation represents 50% of the nominal value.

5.5 Effect of a more refined description of bubble size distribution

The calculations presented so far have been obtained by using a constant and uniform predetermined bubble diameter equal to 0.3 mm. As a second step, simulations have been run using a dedicated model for the bubble-size distribution, namely the Yao & Morel model [13], performed on grid level 2 for run 1.4325. The local distribution of the Sauter diameter of the bubbles in a cross-section is represented in Figure 11, and the profiles of this variables along two directions are shown in Figure 12.

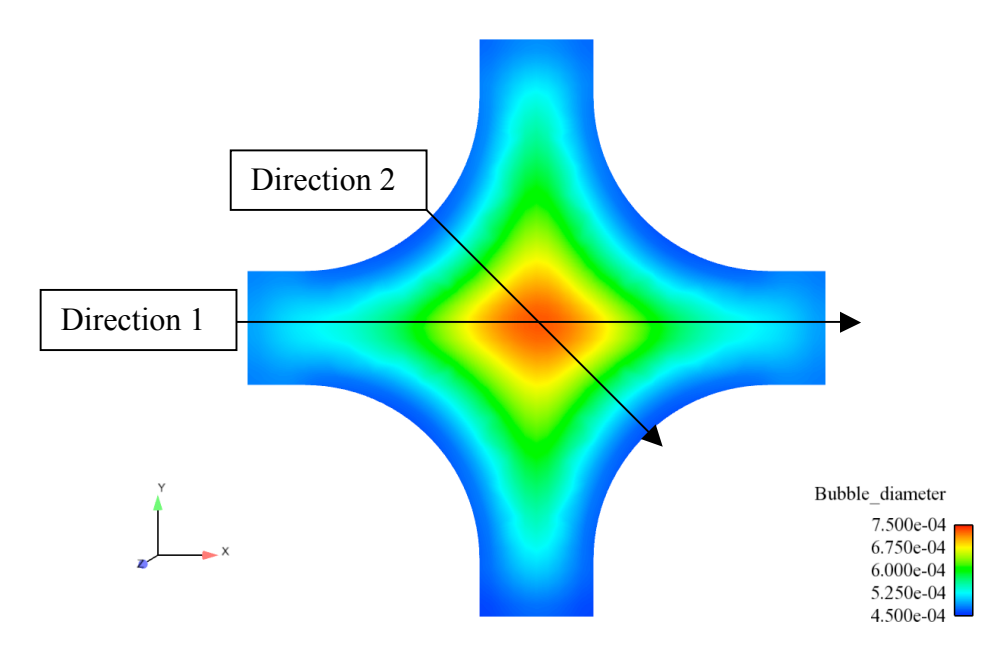
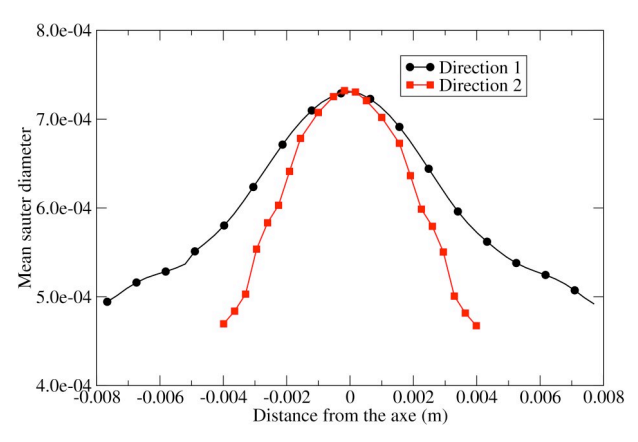


Figure 11 Local distribution of the bubble Sauter diameter at the measuring section (1.40 m from the inlet), using the Yao & Morel model for run 1.4325 on grid level 2.



0.5 - Exp. value Constant diam.

O.4 - Yao & Morel model

0.2 - 0.1 - 0.0 - 0.2 0.4 0.6 0.8 1 1.2 1.4 1.6 1.8 Elevation (m)

Figure 12 Profiles of the calculated mean Sauter diameter of the bubbles along two directions at the measurement section.

Figure 13 Axial evolution of the mean void-fraction for run 1.4325.

In this calculation, the bubble diameter ranges approximately from 0.4 mm to 0.7 mm, the largest bubbles being found in the central region of the domain. It suggests that the choice of a constant diameter of 0.3 mm for the first simulations may have been an underestimation of this parameter for this run. However, the axial evolution of the mean void-fraction plotted in Figure 13 is only slightly impacted by the use of this specific model.

6. Concluding remarks

In this paper, we reported simulations with the multifield CFD code NEPTUNE_CFD in the framework of the first exercise of the OECD NRC PSBT benchmark, which were carried out on a centred, isolated sub-channel geometry and were compared to experimental data. No parameter-tuning of the models applied have been attempted. In nominal conditions, the discrepancy between calculated and experimental mean void-fraction at the measurement section is on average of the order of ±0.05 void-fraction units.

Following the NEA/CSNI Best Practice Guidelines, the impact of the grid on the axial evolution of the mean void-fraction have been investigated by using three grid levels. Furthermore, a study of the numerical propagation of the experimental uncertainties has been carried out, providing an envelope of calculated void-fraction varying from 0.05 to 0.1 around the mean value. This sensitivity analysis could be deepened by sampling all input parameters together, in order to study the coupling between these parameters.

Last, a model allowing to simulate the dispersion in size of the bubbles has been applied for a high void-fraction run, which impacted only slightly the axial evolution of the mean void fraction. As a possible continuation of this work, it would be interesting to further investigate the dependency of the results on the bubble diameter by testing more refined interfacial area models available in NEPTUNE_CFD, and performing as sensitivity study on the bubble size with the fixed bubble-size model.

7. Acknowledgments

This work has been achieved in the framework of the NEPTUNE project, financially supported by CEA (Commissariat à l'Energie Atomique et aux Energies Alternatives), EDF, IRSN (Institut de Radioprotection et de Sûreté Nucléaire) and AREVA-NP.

8. References

- [1] A. Guelfi, D. Bestion, M. Boucker, P. Boudier, P. Fillion, M. Grandotto, J.-M. Hérard, E. Hervieu, P. Péturaud, "NEPTUNE A new software platform for advanced nuclear thermal hydraulics", Nucl. Sci. Eng., Vol. 156, 2007, pp. 281-324
- [2] P. Coste, J. Pouvreau, C. Morel, J. Laviéville, M. Boucker, A. Martin, "Modeling turbulence and friction around a large interface in a three-dimension two-velocity eulerian code", <u>Proceedings of the 12th NURETH conference</u>, Pittsburgh, USA, September 30- October 4, 2007.
- [3] M. Ishii, "Thermo-fluid dynamic, theory of two-phase", Eyrolles, 1975
- [4] N. Mechitoua., M. Boucker., J. Laviéville, J.-M. Hérard, S. Pigny, G. Serre, "An unstructured finite volume solver for two phase water/vapour flows based on an elliptic oriented fractional step method". <u>Proceedings of the 10th Int. Topl. Mtg. Nuclear Reactor Thermal Hydraulics (NURETH 10)</u>, Seoul, Republic of Korea, 2003 October 5–9
- [5] S. Mimouni, F. Archambeau, M. Boucker, J. Laviéville, C. Morel, "A second order turbulence model based on a Reynolds stress approach for two-phase boiling flow. Part 1: Application to the ASU-annular channel case". Nucl. Eng. Des., 2010, Vol. 240, Iss. 9, pp. 2233-2243.
- [6] M. Lance, M. Lopez de Bertodano, "Phase distribution phenomena and wall effects in bubbly two-phase flows". In: Hewitt, G.F., Kim, J.H., Lahey Jr., R.T., Delhaye, J.M., Zuber, N. (Eds.), Multiphase Science and Technology, Vol. 8. Begell House, pp. 69–123., 1994.
- [7] M. Ishii, N. Zuber, "Drag coefficient and relative velocity in bubbly, droplet or particulate flows", AIChE Journal, Vol. 25, No. 5, 1979, pp. 843-855.
- [8] N. Zuber, "On the dispersed two-phase flow in the laminar flow regime". Chemical Engineering Science, Vol. 19, 1964, p. 897.
- [9] A. Tomiyama, H. Tamai, I. Zun, S. Hosokawa, "Transverse migration of single bubbles in simple shear flows", Chemical Engineering Science, Vol 57, Iss. 11, 2002, pp.1849-1858.
- [10] N. Kurul, M. Podowski, "Multidimensional Effects in Forced Convection Subcooled Boiling," <u>Proceedings of the 9th International Heat Transfer Conference</u>, Jerusalem, Israel, 1990 August 19–24, Vol. 1, p. 21.
- [11] S. Mimouni, F. Archambeau, M. Boucker, J. Laviéville, C. Morel, "A second order turbulence model based on a Reynolds stress approach for two-phase boiling flow and

- application to fuel assembly analysis". Nucl. Eng. Des., Vol. 240, Iss. 9, 2010, pp. 2225-2232.
- [12] J.G. Collier, J. R. Thome, "Convective boiling and condensation", Oxford Science Publication, Third Ed., 1994.
- [13] W. Yao, C. Morel, "Volumetric interfacial area prediction in upward bubbly two-phase flow", Int. J. Heat Mass Tran., Vol. 47, Iss. 2, 2004, pp 307-328.